Available online at www.sciencedirect.com
ScienceDirect
International Journal of Solids and Structures 45 (2008) 3793–3806
INTERNATIONAL JOURNAL OF SOLIDS AND STRUCTURES
www.elsevier.com/locate/ijsolstr

Stability and shape evolution of voids and channels due to surface misfit

David Salac, Wei Lu *

Department of Mechanical Engineering, University of Michigan, Ann Arbor, MI 48109, USA

Received 1 June 2007; received in revised form 14 October 2007
Available online 30 October 2007

Abstract

This paper investigates the stability and shape evolution of voids and channels under the combined effects of surface misfit, surface energy and surface diffusion. A dynamic model that incorporates the competition among these energetic forces is developed. Our approach integrates a novel local semi-implicit level set method to capture interface movement and an iterative spectral method to calculate the elastic field, which allows simulating very large shape evolution such as void breakup or coalescence in a wide range of materials systems. Our study reveals the important effect of surface misfit and remarkably rich dynamics during shape evolution. It is shown that surface misfit can lead to instabilities of voids, break-up of channels and ordering of voids.

Keywords: Surface misfit; Surface diffusion; Self-assembly

1. Introduction

Elasticity has been shown to influence the stability and morphology of voids (Siegel et al., 2004; Tvergaard and Hutchinson, 2002; Wang and Suo, 1997; Wu, 1999). A common example is voids in a solid subjected to externally applied loads. These voids may change their shape to accommodate the loading, changing from circular to elliptical shapes, or developing cusps (Siegel et al., 2004; Wang and Suo, 1997). While many studies have focused on elasticity in a bulk material, recently work suggests that surface elastic effect, such as surface stress, can play an important role in morphological changes. For instance, a flat surface may become unstable due to surface stress when the wavelength of perturbation is larger than a critical value (Wu et al., 1998). Surface stress can also lead to phase separation on a solid surface (Lu and Kim, 2005; Lu and Suo, 2001, 2002). One aspect that has not received much attention is that of the surface elastic effect on a moveable surface which undergoes large shape change. Atoms on a material surface have different bonding situations from those inside the material. This effect causes the

* Corresponding author. Tel.: +1 734 647 7858; fax: +1 734 647 3170.
E-mail address: weilu@umich.edu (W. Lu).

0020-7683/$ - see front matter © 2007 Elsevier Ltd. All rights reserved.
doi:10.1016/j.ijsolstr.2007.10.018

atoms on the surface to have a different lattice constant, leading to a misfit localized in a thin surface layer. This paper aims to develop a model to investigate the stability and shape evolution of voids and channels under surface misfit.

An understanding of how voids and channels evolve is critical to the reliability of small scale devices. For example, electromigration has been known to cause failure in electronic interconnects (Arzt et al., 1994; Riege et al., 1995; Stahlmecke et al., 2006). Driven by the electron wind, voids may change their shape via surface diffusion. Depending on the initial void shape, the resulting change can lead to a slit forming either along the line, which does not cause circuit breakage, or across the line, which causes the line to fail (Wang and Suo, 1996). The two situations classify the initial void shapes into two categories: non-critical and critical. However, surface misfit and the shape change it drives may change the result of electromigration: it may drive a non-critical void into a critical one or vice versa.

Morphological change of voids can also affect the behavior of bulk materials. It is well known that cracks may initiate at void interfaces when the bulk material is under external loadings (Newcomb and Tressler, 1993). It also is known that there exists a critical stress level on the void interface for these cracks to form, and that these cracks can lead to structural failure (McCartney, 1977; Stevens and Dutton, 1971). What has not received enough attention is that even if the applied load is not sufficient to cause void shape changes, surface misfit in the system can lead to high stress regions on the void surface, allowing cracks to form which might otherwise not be possible.

On the other hand, small scale defects formed in a controllable manner may be used for nanofabrication. When a thin film is cracked and the crack is subsequently filled with appropriate materials, nanowires with very high aspect ratios can be made (Alaca et al., 2004). It has also been shown that cracking can be directed to fabricate nanowire patterns (Salac and Lu, 2006). This concept may be applied to voids and channels. For example, it is known that a channel may break into multiple voids through the Rayleigh instability (Glaeser, 2001). While the Rayleigh instability only deals with the surface energy, elastic effects can also influence the stability of defects (Colin, 2007). An understanding of how the surface misfit affects the resulting structures could allow for the creation of extremely small scale yet highly regular structures. An example of this would be the creation of regularly spaced voids from the breakup of a long channel. These voids may further be used as a template to create regularized nanodots.

The organization of this article is as follows. Section 2 will introduce the model to capture large shape evolution of voids and channels. The application of a spectral elastic field calculation, coupled with a novel local semi-implicit level set formulation to advance the interface, allows for accurate simulations over a long time. Representative results, such as stability of a void, breakup of channels and interaction of multiple voids will be presented in Section 3. Section 4 is a brief concluding remarks.

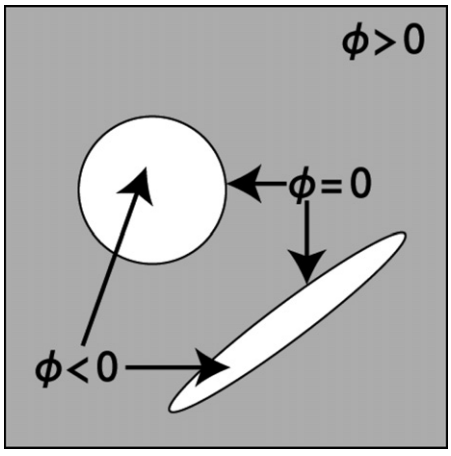

Fig. 1. The level set description of voids and channels in a solid.

2. Modeling of shape evolution

Consider an otherwise homogeneous solid containing voids and channels, as shown in Fig. 1. The motion of surfaces is driven by the minimization of the chemical potential along the surfaces. The chemical potential μ can be broken down into two components:

$$\mu = \mu_s + \mu_e, \tag{1}$$

where μ_s is the contribution from the surface energy, and μ_e the contribution from the elastic effect. Allow the surface to evolve through surface diffusion. Assume that the mass flux on the surface is proportional to the driving force, i.e. the surface gradient of the chemical potential. This kinametic relation together with mass conservation gives the normal velocity of the surface, V_n, which is

$$V_n = \frac{D}{\Omega}\nabla_s^2\mu. \tag{2}$$

Here Ω is the atomic volume, ∇_s^2 the surface Laplacian, and D a diffusion coefficient (Siegel et al., 2004).

The chemical potential due to surface energy is given by

$$\mu_s = \Omega\gamma\kappa, \tag{3}$$

with γ the surface energy density and κ the local curvature (Wu et al., 1998; Yang, 2006).

The chemical potential due to the elastic field is given by

$$\mu_e = -\Omega\frac{1}{2}\lambda_{ijkl}(\varepsilon_{ij} - \varepsilon^0_{ij})(\varepsilon_{kl} - \varepsilon^0_{kl}), \tag{4}$$

where λ_{ijkl} is the elastic stiffness tensor, ε_{ij} the local strain and ε^0_{ij} the local misfit strain.

Eqs. (1)–(4) completely describe the surface motion. Choose a characteristic strain ε_m, stiffness E and length l_0. Define a characteristic velocity by

$$V_0 = \frac{D\gamma}{l_0^3}. \tag{5}$$

Normalize strain by ε_m, elastic stiffness by E, length by l_0 and surface velocity by V_0. The dimensionless surface evolution equation is given by

$$V_n = \nabla_s^2\left(\kappa - \frac{\Lambda}{2}\lambda_{ijkl}(\varepsilon_{ij} - \varepsilon^0_{ij})(\varepsilon_{kl} - \varepsilon^0_{kl})\right). \tag{6}$$

Here ∇_s^2 and κ are dimensionless surface Laplacian and curvature, respectively. The dimensionless parameter Λ measures the importance of elasticity relative to that of surface energy, which is defined by

$$\Lambda = \frac{E\varepsilon_m^2 l_0}{\gamma}. \tag{7}$$

2.1. Spectral elastic field calculation

The potential due to elasticity in Eq. (4) requires information of the elastic field. Specifically, we need to consider the elastic field in a solid containing voids and channels with complicated elastic interactions among them. Here we apply an iterative spectral method. The key idea is to consider the entire solid as a non-uniform body with position-dependent elastic stiffness and misfit. Voids and channels are treated implicitly by assigning zero stiffness. This general approach can treat voids and channels with arbitrary geometries.

The elastic stiffness at any given point in the void-solid composite can be related to the stiffness of the solid through a density-like function (Yu and Lu, 2005),

$$\lambda_{ijkl}(\mathbf{x}) = (1 - \rho_\lambda(\mathbf{x}))\lambda^B_{ijkl}. \tag{8}$$

Here $\mathbf{x}$ is the position vector, λ^B_{ijkl} the solid stiffness and $\rho_\lambda(\mathbf{x})$ a density function which smoothly transitions from a value of 1 inside the void to a value of 0 in the solid. A continuous $\rho_\lambda(\mathbf{x})$ is for computational convenience. The specific form is insignificant as long as the transition is narrow.

The lattice misfit between the surface atoms and those inside the solid is taken to have the form of

$$\varepsilon^0_{ij}(\mathbf{x}) = \rho_\varepsilon(\mathbf{x})\varepsilon_0\delta_{ij}, \tag{9}$$

where $\rho_\varepsilon(\mathbf{x})$ is another density-like function varying between 0 and 1, which controls the decay of the misfit strain from the surface to the solid, and ε_0 is a constant that measures the magnitude of misfit. The form of $\rho_\varepsilon(\mathbf{x})$ is independent of $\rho_\lambda(\mathbf{x})$.

The elastic field of the non-uniform solid can be expressed by the supposition of a uniform field and an inhomogeneous perturbation field. The total strain field, $\varepsilon_{ij}(\mathbf{x})$, is expressed as

$$\varepsilon_{ij}(\mathbf{x}) = \tilde{\varepsilon}_{ij}(\mathbf{x}) + \bar{\varepsilon}_{ij}, \tag{10}$$

where $\bar{\varepsilon}_{ij}$ is the uniform strain and $\tilde{\varepsilon}_{ij}(\mathbf{x})$ the inhomogeneous strain. The homogeneous strain is the uniform macroscopic strain characterizing the macroscopic shape and volume change associated with the total strain. It relates to the macroscopic applied stress by the volume average of the system stiffness. When there is no external load applied on the solid the macroscopic strain $\bar{\varepsilon}_{ij}$ reduces to zero. The inhomogeneous strain, $\tilde{\varepsilon}_{ij}(\mathbf{x})$, relates to the perturbation displacement, $u_i(\mathbf{x})$, by

$$\tilde{\varepsilon}_{ij}(\mathbf{x}) = \frac{1}{2}\left(\frac{\partial u_i(\mathbf{x})}{\partial x_j} + \frac{\partial u_j(\mathbf{x})}{\partial x_i}\right). \tag{11}$$

The total stress field, $\sigma_{ij}(\mathbf{x})$, can be computed with

$$\sigma_{ij}(\mathbf{x}) = \lambda_{ijkl}(\mathbf{x})[\varepsilon_{kl}(\mathbf{x}) - \varepsilon^0_{kl}(\mathbf{x})]. \tag{12}$$

The elastic field reaches equilibrium much faster than material diffusion along the void surface. Thus the elastic field satisfies the standard elastic equilibrium equation,

$$\frac{\partial \sigma_{ij}(\mathbf{x})}{\partial x_j} = 0. \tag{13}$$

Substituting Eqs. (10)–(12) into Eq. (13), we obtain a partial differential equation for the displacement field,

$$\frac{\partial}{\partial x_j}\left\{\lambda_{ijkl}(\mathbf{x})\left[\frac{\partial u_k(\mathbf{x})}{\partial x_l} + \bar{\varepsilon}_{kl} - \varepsilon^0_{kl}(\mathbf{x})\right]\right\} = 0. \tag{14}$$

To ensure numerical stability, we add a term of $-A_{ijkl}\,\partial^2 u_k/\partial x_j\partial x_l$ to both sides of Eq. (14), where A_{ijlm} is a chosen constant for computational stability. Rearranging the terms gives

$$-A_{ijkl}\frac{\partial^2 u_k(\mathbf{x})}{\partial x_j \partial x_l} = \frac{\partial}{\partial x_j}\left\{\lambda_{ijkl}(\mathbf{x})\left[\bar{\varepsilon}_{kl} - \varepsilon^0_{kl}(\mathbf{x})\right] + \left[\lambda_{ijkl}(\mathbf{x}) - A_{ijkl}\right]\frac{\partial u_k(\mathbf{x})}{\partial x_l}\right\}. \tag{15}$$

Take the Fourier transform of Eq. (15) and solve the equation by iteration. The displacement field is given by

$$\hat{u}^{(n)}_p(\mathbf{k}) = \sqrt{-1}G_{ip}(\mathbf{k})k_j\left\{\lambda_{ijlm}(\mathbf{x})[\bar{\varepsilon}_{lm} - \varepsilon^0_{lm}(\mathbf{x})] + [\lambda_{ijlm}(\mathbf{x}) - A_{ijlm}]\frac{\partial u^{(n-1)}_l(\mathbf{x})}{\partial x_m}\right\}_{\mathbf{k}}, \tag{16}$$

where $\mathbf{k}$ is the wave vector in Fourier space and $G_{ip}(\mathbf{k}) = (A_{ijpm}k_jk_m)^{-1}$ is the Green's tensor. The hat or a subscript '$\mathbf{k}$' denotes Fourier Transform. The initial value is taken to be $\hat{u}^{(0)}_p(\mathbf{k}) = \sqrt{-1}G_{ip}(\mathbf{k})k_j\{\lambda_{ijlm}(\mathbf{x})[\bar{\varepsilon}_{lm} - \varepsilon^0_{lm}(\mathbf{x})]\}_{\mathbf{k}}$. The gradient, $\partial u^{(n-1)}_l(\mathbf{x})/\partial x_m$, is obtained by inverse Fourier transform of $\sqrt{-1}k_m\hat{u}^{(n-1)}_l(\mathbf{k})$. The convergence of Eq. (16) depends on the choice of A_{ijlm}. We chose $A_{ijlm} = \lambda^B_{ijlm}$, and found that Eq. (16) converges after about 10 iterations. After the displacement field is obtained, the strain field can be calculated by Eq. (11) with Fourier transform on both sides and then inverse Fourier transform.

2.2. Local, semi-implicit level set scheme for advancing interfaces

The level set method has recently become an invaluable tool for investigating the motion of interfaces in a wide variety of systems and situations. The method has successfully been employed to investigate electromigration (Li et al., 1999), epitaxial growth (Chen et al., 2001) and evolving fluid interfaces (Sethian and Smereka, 2003). While useful, the basic level set method is hampered by relatively high computational costs, especially in situations concerning surface diffusion. To relieve this constraint, two different classes of approaches have been developed. The first aims to reduce the overall computational cost by localizing the level set calculation, known as the local level set method (Peng et al., 1999). The second aims at developing semi-implicit schemes to increase the temporal stability so that larger time steps can be utilized (Smereka, 2003). In this paper, we demonstrate the first use of a novel hybrid level set method that combines the numerical efficiency of the local level set approach with the temporal stability afforded by a semi-implicit method.

First introduced by Osher and Sethian (1988), the central concept of the level set approach is to describe an interface, Γ, implicitly by embed it into a function of higher dimensionality, ϕ. The interface is given by the zero level-set of ϕ, i.e.

$$\Gamma(t) = \{\mathbf{x} | \phi(\mathbf{x}, t) = 0\}, \tag{17}$$

where $\mathbf{x}$ is a position vector and t is time. To describe a void in a solid, we can define the level set function ϕ such that

$$\phi(\mathbf{x}, t) \begin{cases} < 0 \text{ in void}, \\ = 0 \text{ on } \Gamma(t), \\ > 0 \text{ in bulk}, \end{cases} \tag{18}$$

as shown in Fig. 1. Using this level set formulation, the normal of the interface, $\mathbf{n}$, is given by

$$\mathbf{n} = \frac{\nabla \phi}{|\nabla \phi|}. \tag{19}$$

The positive normal direction points outward of the void, i.e. from the region of negative to positive $\phi(\mathbf{x}, t)$. The curvature of the surface, κ, is given by the divergence of the normal (Peng et al., 1999),

$$\kappa = \nabla \cdot \frac{\nabla \phi}{|\nabla \phi|}. \tag{20}$$

The curvature is positive for a convex void surface.

While any function that satisfies Eq. (18) can be a valid choice for ϕ, it is advantageous to choose specific forms with known properties. Here we use the signed distance function. By definition a signed distance function describes the shortest distance from any given point in space to the interface, with a positive value on one side of the interface (solid) and a negative value on the other side (void).

The motion of the interface carries the associated $\phi(\mathbf{x}, t)$ field in a way similar as a flow that carries mass. Denote the interface velocity by $\mathbf{V}$ and consider a control volume, it is easy to show that

$$\frac{\partial \phi}{\partial t} + \mathbf{v} \cdot \nabla \phi = 0. \tag{21}$$

The interface velocity can be decomposed into components normal ($V_n \mathbf{n}$) and tangential ($V_t \mathbf{t}$) to the interface. As $\mathbf{t} \cdot \nabla \phi = \mathbf{0}$, Eq. (21) can be rewritten in the form of the standard evolution equation,

$$\frac{\partial \phi}{\partial t} + V_n |\nabla \phi| = 0 \tag{22}$$

The interface motion is determined by calculating the normal velocity of the interface using Eq. (6) and advancing the level-set function using Eq. (22).

The main difficulty in advancing the level-set function using the normal velocity as given in Eq. (6) is that the resulting differential equation is extremely stiff. In fact, solving this level set evolution equation is analogous to solving the fourth-order differential equation $\phi_t = -\phi_{xxxx}$. Any explicit time-discretization method

will require that the time step scale as Δx^4, where Δx is the grid spacing. Clearly this is a very stringent condition. To reduce this restriction we propose a local, semi-implicit level set method.

The key idea is to reformulate Eq. (22) into a semi-implicit equation where a linear portion can be integrated implicitly and the non-linear portion is integrated explicitly. This can be done by adding a bilaplacian stabilization term to both sides:

$$\frac{\partial \phi}{\partial t} + \beta \nabla^4 \phi = \beta \nabla^4 \phi - V_n |\nabla \phi|, \tag{23}$$

with β a positive constant. By writing the time differential to first-order accuracy, implicitly calculating the left hand bilaplacian and explicitly calculating the right hand terms we obtain the discrete form of Eq. (23),

$$(1 + \Delta t \beta \nabla^4) \delta \phi^{n+1} = -\Delta t V_n |\nabla \phi^n|. \tag{24}$$

Here Δt is the time step, ϕ^n is the level set function at time t, $\delta \phi^{n+1} = \phi^{n+1} - \phi^n$ are the level-set updating values, and ϕ^{n+1} is the level set function at time $t + \Delta t$. The bilaplacian term acts as a smoothing operator applied to an explicit scheme, suppressing the unstable high wave number modes. This approach allows for the use of larger time steps than explicit methods without loss of stability. A similar method has been applied to phase-field models (Lu and Salac, 2005; Suo and Hong, 2004).

To reduce the overall computational time, we localize all level set calculations to a small region around the interface (Chopp and Sethian, 1999; Khenner et al., 2001; Peng et al., 1999). Begin by considering two arbitrary two-dimensional voids on a Cartesian grid with uniform grid spacing, as shown in Fig. 2a. Let $0 < \alpha < \beta$ be two constants on the order of the grid spacing. Mark all grid points within a distance of α from the surface in a calculation tube Γ_α. Define a similar tube, Γ_β, for all points within a distance of β from the surface and not in Γ_α. The void surface and surface dependent quantities such as curvature are calculated within these tubes.

The simplest implementation of a local semi-implicit level set scheme would be to update all points in Γ_α and Γ_β using Eq. (24) for each time step. We have tried this implementation and observed interface distortion and poor temporal stability when two voids are close. The reason is that a straight discretization of Eq. (24) results in a 5×5 stencil in two-dimensions, which allows for surface information to leak from one void to another before they are actually in touch with each other. This effect causes problems to accurately simulate void coalescence.

To ensure that as little surface information as possible is leaked between voids, we perform an extraction step. Here each void is extracted into a temporary level set function. This extracted void has the same interface as the original. We then construct a temporary signed distance function based on this extracted interface using a third-order weighted essentially non-oscillatory (WENO3) upwind reinitialization scheme to all grid points

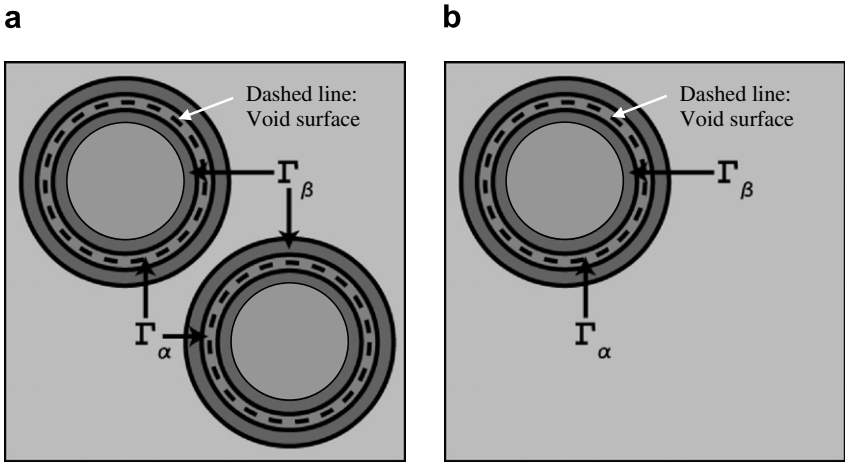

Fig. 2. (a) The calculation tubes for a sample system. (b) The extracted void and the two surrounding calculation tubes. Physical quantities such as curvature are calculated using this temporary, extracted, level set function.

in Γ_α and Γ_β (Jiang and Peng, 2000). Any values intrinsic to the interface, such as curvature, are not affected through this extraction process (Adalsteinsson and Sethian, 1999). Fig. 2b illustrates the step.

Following (Smereka, 2003), we use the temporary level set function, $\tilde{\phi}$, to calculate the chemical potential at grid points directly next to the interface. The potential information is then extended by at least 2 grid points away from the interface. Using the extended potential it is possible to calculate the normal velocity through Eq. (6) at grid points next to the interface. This is followed by an extension of V_n to Γ_α and Γ_β. We then calculate $\Delta t v_n |\nabla \tilde{\phi}|$ in Γ_α and Γ_β using an upwind WENO3 scheme (Jiang and Peng, 2000). The next step is to solve for $\delta\phi^{n+1}$ in the system of equations defined by Eq. (24) using the BI-CGSTAB method (Vandervorst, 1992). Recall that the value of β was explicitly set to be larger than α. This allows us to use the points within Γ_β as boundary conditions for calculating the smoothed updating values in Γ_α. The smoothed updating values using the extracted level set are used to update the main level set function describing the original system.

There are some comments about the form chosen for the bilaplacian stabilization term added to Eq. (24). The simplest form would be to use central differences to calculate all the directional derivatives, resulting in an anisotropic stencil (Patra and Karttunen, 2006). We have found that using this discretization is not optimal. Instead we utilize an isotropic stencil which should aid in the stability of the simulation. In particular we utilize the second order isotropic bilaplacian stencil given by Patra and Karttunen (2006).

Finally, we specify the specific density forms for the stiffness, Eq. (8), and the misfit strain, Eq. (9). We would like to utilize density functions which depend on the distance to the nearest void, and the level set function easily allows for such functions. In both cases, we require a smooth transition from material properties inside the void to the solid over a known thickness. In this work we have chosen the following density function:

$$\rho(\phi) = \frac{1}{2}\left[1 - \tanh\left(4.59512\frac{\phi - h_1}{h_2 - h_1} - 2.29756\right)\right]. \tag{25}$$

Here h_1 and h_2 control the distance from the surface where the function goes from 1 to 0, with $h_1 < h_2$. This particular function has the property of being greater than 0.99 if $\phi < h_1$ and less than 0.01 if $\phi > h_2$. Varying these two control parameters allows us to specify two different density profiles for the stiffness and the surface misfit.

3. Results

The numerical algorithm shown in Section 2 has been implemented to study various configurations of voids and channels in a solid. Unless otherwise noted the following are the material parameters used. Consider solids with cubic structures. The normalized stiffness values are taken to be $C_{11} = 3$, $C_{12} = 1$ and $C_{44} = 1$ (elastic isotropic). The transition from zero stiffness of void to the stiffness of solid is given by Eq. (25). We take $h_1 = -2.0$ and $h_2 = 0.0$. We take the characteristic strain ε_m to be $|\varepsilon_0|$ and assume a negative misfit, which gives $\varepsilon_0/\varepsilon_m = -1$. The misfit is localized in a thin layer close to the surface. To do this we use the density form given by Eq. (25) and set $h_1 = -2.0$, $h_2 = 2.0$ and replace ϕ by $|\phi|$. This choice essentially ensures full normalized misfit (-1) at the surface and decaying to zero as one moves away from the surface. All calculations shown below are done on a uniform Cartesian grid with a spacing of 0.5. Time steps as large as 1.0 were utilized, with the time step being reduced as necessary to capture any rapid configuration changes.

3.1. Circular voids

The stability and shape change of circular voids under elastic effects has caused many interests (Colin, 2007; Wang and Suo, 1997; Wu, 1999). Previous works have indicated that stretching a film with a hole in the center to a certain stress level may cause it to perturb away from a circular shape (Colin, 2007). We find that surface misfit can lead to similar phenomenon. Fig. 3 shows the evolution of an initially circular void with a radius of 20 up to a time of 250 with $\Lambda = 4.0$. To facilitate the discussion, we define the growth mode by R/N, where R is the initial radius of the void and N the number of perturbations on the surface. This number is directly related to the perturbation wavelength. The early stage growth (Fig. 3b and c) is primarily the $R/N = 20/8 = 2.5$ mode. For longer times a shorter wavelength mode, $R/N = 1.67$, begins to dominate, as seen in Fig. 3d. This result is consistent with theoretical investigations of void surfaces under externally applied loadings (Colin, 2007).

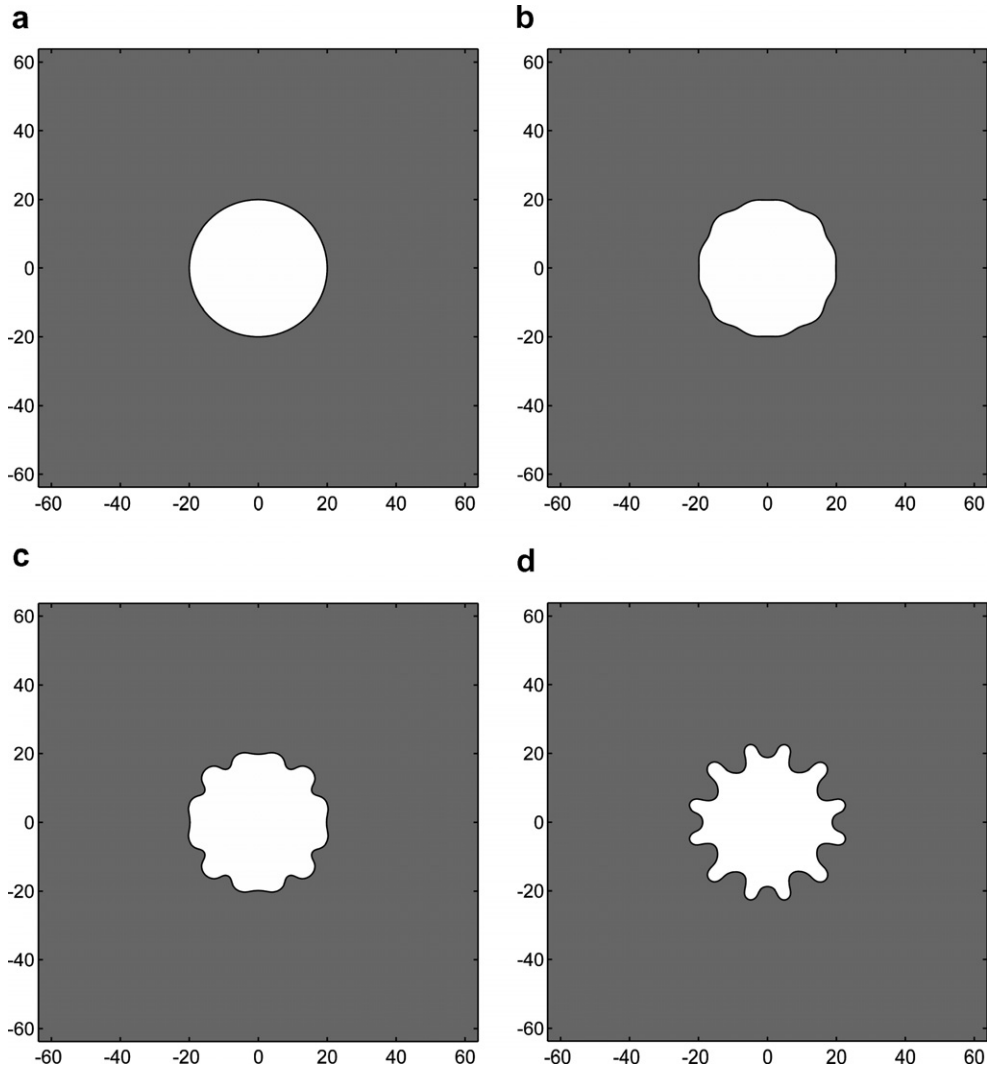

Fig. 3. Evolution of an initially circular void with radius of 20 and $\Lambda = 4.0$. Shown for times of (a) 0, (b) 38, (c) 50 and (d) 250. The early-time evolution is characterized by a growth mode of $R/N = 2.5$ while the fastest long-time growth mode is $R/N = 1.67$.

Next we investigate the influence of initial void size on surface stability. Consider three initially circular voids of radius 20, 30 and 40 under $\Lambda = 4.0$, which is strong enough to induce instabilities in all three cases. The resulting surfaces at a time of 250 are shown in Fig. 4. Here the dominant long-term growth modes are: $R/N = 1.67$ for $R = 20$, $R/N = 1.875$ for $R = 30$ and $R/N = 1.67$ for $R = 40$. The discrepancy between the $R = 30$ and the $R = 20$ and $R = 40$ voids can be attributed to the discrete nature of the perturbations allowed on the interface.

This relationship between the fastest long-term growth mode and the strength of surface misfit is given in Fig. 5. Here the misfit strength varies from $\Lambda = 0.5$ to $\Lambda = 8.0$. In all cases as the misfit becomes stronger and begins to dominate, the fastest growth mode decreases, indicating that the wavelength decreases.

3.2. Channels

In addition to voids, the evolution and stability of channels has been of many interests (Glaeser, 2001; Nichols, 1976). Here we consider the instability and eventual breakup of channels with the surface misfit effect.

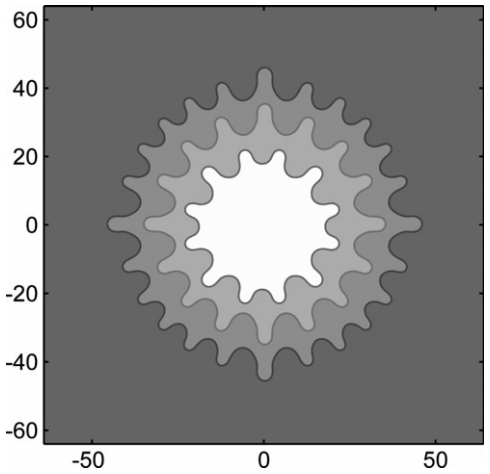

Fig. 4. Profile of three initially circular voids under $\Lambda = 4.0$ and at time 250. Inner void has radius of 20, middle void radius of 30, outer void radius of 40. The fastest long-term growth modes are $R/N = 1.67$ ($R = 20$), $R/N = 1.875$ ($R = 30$) and $R/N = 1.67$ ($R = 40$). The difference in the growth mode can be attributed to the discrete nature of the perturbations allowed on the surface.

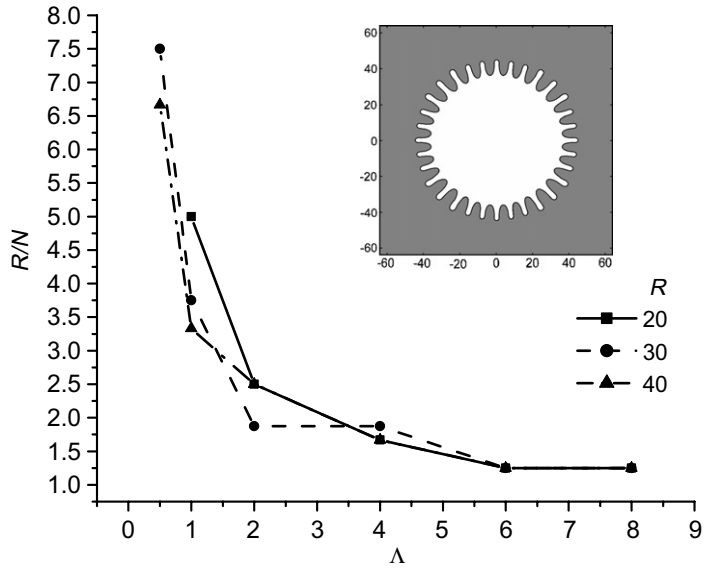

Fig. 5. The observed fastest growth mode for initially circular voids of radius 20, 30 and 40. In general as surface misfit becomes stronger, the growth mode (and thus the wavelength) decrease. The insert demonstrates the saturated growth mode for $R = 40$ and $\Lambda = 8.0$ at a time of 50.

First consider a single channel with half-width of $R = 3$ and length of $l = 60$ as shown in Fig. 6. The evolution of this channel under two different misfits are shown, with $\Lambda = 2.0$ seen in Fig. 6a–e and $\Lambda = 4.0$ seen in Fig. 6f–j. Due to surface misfit, any initial perturbations are amplified (Fig. 6b and g). These amplified perturbations eventually result in a pinching-off from the ends of the channel (Fig. 6c and h). The result is a series of voids, each approximately equal in volume, aligned along the original channel axis (Fig. 6e and j). Note that due to the presence of multiple voids, elastic interactions through the solid causes the voids at the center to develop a slit-like shape perpendicular to the original channel direction. This is in contrast to the voids at the outer edges of the original channel, which take on a more rounded shape. The resulting shapes should be contrasted with the result obtained in the absence of elastic

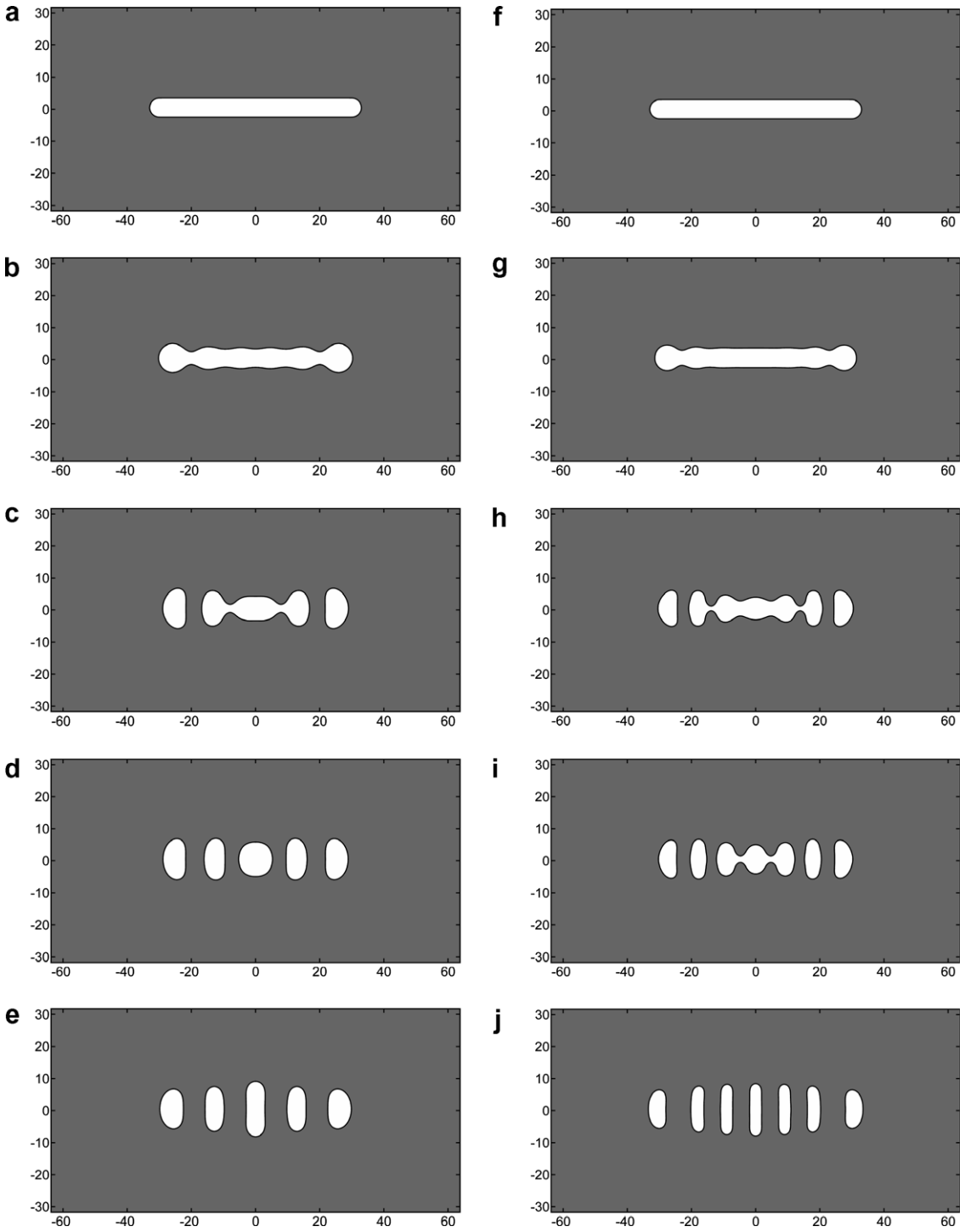

Fig. 6. Evolution of a channel with half-width of 3 and length of 60 under two different surface misfits. Times are the following. (a) 0, (b) 50, (c) 100, (d) 125, (e) 500 for $\Lambda = 2.0$. (f) 0, (g) 12.5, (h) 25, (i) 30, (j) 500 for $\Lambda = 4.0$. Stronger misfit induces a shorter wavelength mode, resulting in smaller voids closer together. In the absence of surface misfit the channel would evolve into a single, large circular void.

effects. In this case the channel will evolve into a single void, which agrees with the experimental result for finite aspect ratio pore channels (Glaeser, 2001).

3.3. Multiple voids and anisotropy

Here we present results for a system of multiple voids, which can be observed in porous media or during the annealing of materials (Colin, 2007). In these results the periodicity of the system is exploited to allow for the simulation of large systems through the use of a characteristic volume. Consider a system consisting of 16 voids randomly placed in a bulk, Fig. 7a. We observe the evolution and final equilibrium position of the voids when $\Lambda = 1.0$, Fig. 7b–d. As can be seen, the elastic interactions induce the voids to migrate from their initial positions. After a time of 750 the voids have moved into a cubic structure, aligning along the horizontal and vertical directions. Simultaneously the voids undergo a shape change, from their initially circular shape to a much more oblong shape. It is interesting to note that long axis of the voids alternates in this situation.

Finally, we consider anisotropic elastic effects on the structure of multiple voids. Here we take a small region of the bulk containing nine, initially circular voids. We show this in Fig. 8a, replicating the periodic pattern to aid in pattern recognition. Here we allow the system to evolve under the influence of a strong misfit, $\Lambda = 4.0$, up to a time of 1000. When the anisotropy ratio $A = 2C_{44}/(C_{11} - C_{22}) - 1$, is negative by setting $C_{11} = 3$, $C_{12} = 1$, $C_{44} = 0.25$ ($A = -0.75$), the resulting pattern is similar to Fig. 7. For this elastic anisotropy the compliant direction is the vertical and horizontal direction. Due to the anisotropy we do not obtain the

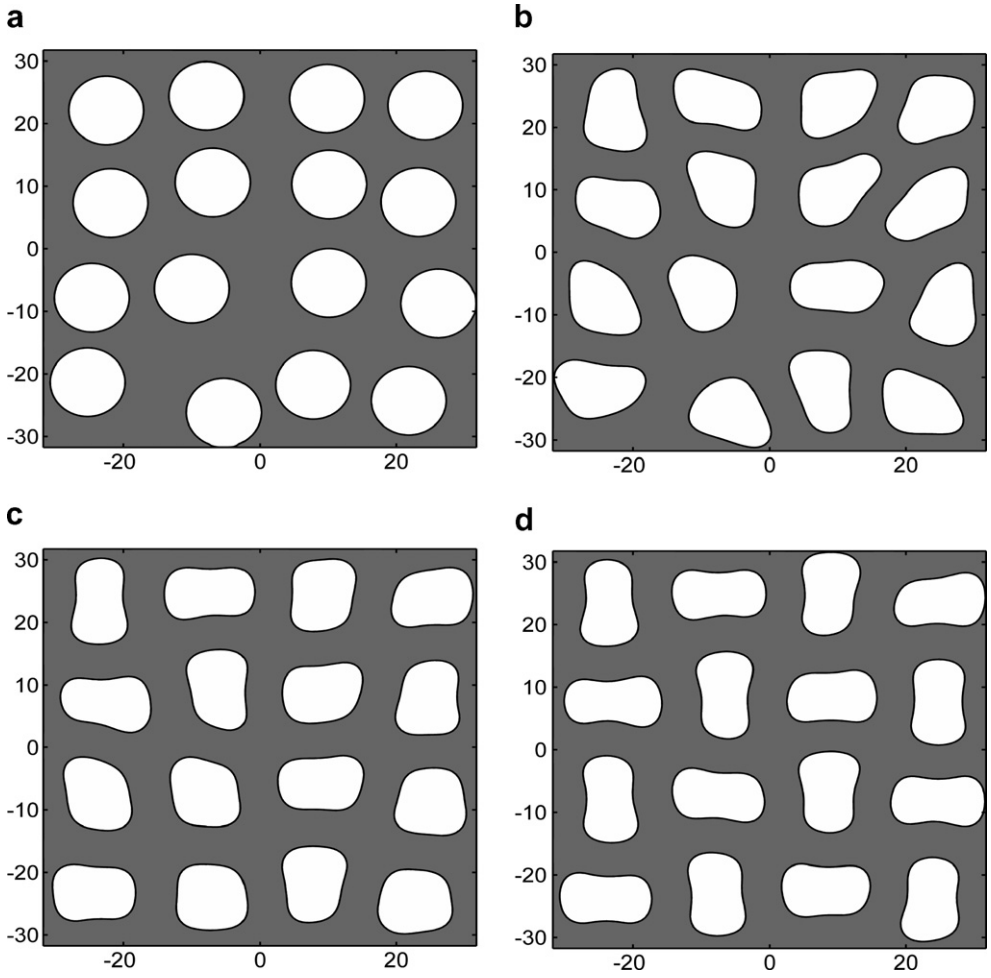

Fig. 7. Evolution of many voids with random initial positions. Surface misfit is $\Lambda = 1.0$. Shown for times (a) 0, (b) 25, (c) 250, (d) 750. The resulting pattern is much more uniform than the original pattern.

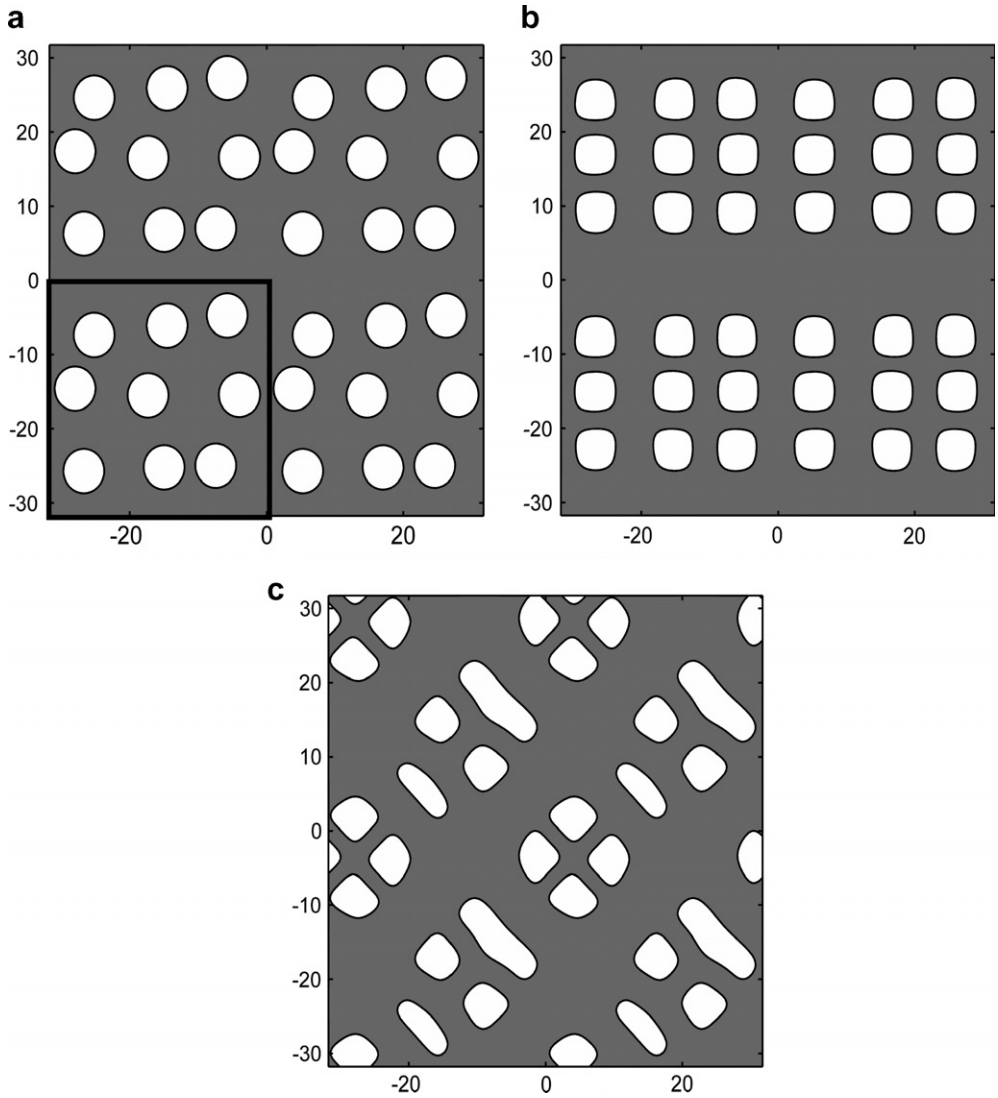

Fig. 8. Void patterns at time 1000 for systems with various elastic anisotropy, A, and surface misfit $\Lambda = 4.0$ (a) The initial void distribution. The periodic nature of the system is exploited by only calculating in a small region, shown by the black outline in (a). Normalized elastic constants are: (b) $C_{11} = 3$, $C_{12} = 1$, $C_{44} = 0.25$ ($A = -0.75$) and (c) $C_{11} = 3$, $C_{12} = 1$, $C_{44} = 2$ ($A = 1.0$).

oblong structure seen in the previous result, but obtain voids much more uniform in size and orientation. This result should be contrasted with the case of a positive anisotropy ratio given by setting $C_{11} = 3$, $C_{12} = 1$, $C_{44} = 2$ ($A = 1.0$). In this case the elastic compliant direction follows the diagonals, which leads to the pattern aligning along these directions. A multi-level ordering also occurs, with a small number of voids (4–6) forming a sub-unit of the overall structure. Note that in this case we obtain void coalescence, which results in the observed elongated voids.

4. Concluding remarks

This paper provides an understanding of how surface misfit affects the stability and shape of voids and channels. The application of an iterative, spectral elastic field calculation coupled with a novel local, semi-implicit level set formulation allows for the accurate simulation of void and channel evolution for long periods of time. Our study reveals the important effect of surface misfit on shape evolution and the dynamic process

that it leads to instabilities of voids, break-up of channels and ordering of voids. Consideration of surface misfit may lead to better prediction of device reliability or novel nanofabrication approaches.

Acknowledgement

The authors acknowledge financial support from National Science Foundation CAREER Award No. DMI-0348375.

References

Adalsteinsson, D., Sethian, J.A., 1999. The fast construction of extension velocities in level set methods. Journal of Computational Physics 148, 2–22.

Alaca, B.E., Sehitoglu, H., Saif, T., 2004. Guided self-assembly of metallic nanowires and channels. Applied Physics Letters 84, 4669–4671.

Arzt, E., Kraft, O., Nix, W.D., Sanchez, J.E., 1994. Electromigration failure by shape change of voids in bamboo lines. Journal Of Applied Physics 76, 1563–1571.

Chen, S., Merriman, B., Kang, M., Caflisch, R.E., Ratsch, C., Cheng, L.T., Gyure, M., Fedkiw, R.P., Anderson, C., Osher, S., 2001. A level set method for thin film epitaxial growth. Journal of Computational Physics 167, 475–500.

Chopp, D.L., Sethian, J.A., 1999. Motion by intrinsic Laplacian of curvature. Interfaces and Free Boundaries 1, 1–18.

Colin, J., 2007. On the surface stability of a spherical void embedded in a stressed matrix. Journal of Applied Mechanics-Transactions of the Asme 74, 8–12.

Glaeser, A.M., 2001. Model studies of Rayleigh instabilities via microdesigned interfaces. Interface Science 9, 65–82.

Jiang, G.S., Peng, D.P., 2000. Weighted ENO schemes for Hamilton–Jacobi equations. Siam Journal on Scientific Computing 21, 2126–2143.

Khenner, M., Averbuch, A., Israeli, M., Nathan, M., 2001. Numerical simulation of grain-boundary grooving by level set method. Journal of Computational Physics 170, 764–784.

Li, Z.L., Zhao, H.K., Gao, H.J., 1999. A numerical study of electro-migration voiding by evolving level set functions on a fixed Cartesian grid. Journal of Computational Physics 152, 281–304.

Lu, W., Kim, D., 2005. Engineering nanophase self-assembly with elastic field. Acta Mater 53, 3689–3694.

Lu, W., Salac, D., 2005. Programmable nanoscale domain patterns in multilayers. Acta Materialia 53, 3253–3260.

Lu, W., Suo, Z., 2001. Dynamics of nanoscale pattern formation of an epitaxial monolayer. Journal of the Mechanics and Physics of Solids 49, 1937–1950.

Lu, W., Suo, Z., 2002. Symmetry breaking in self-assembled monolayers on solid surfaces. I. Anisotropic surface stress. Physical Review B 65, 085401.

McCartney, L.N., 1977. Cavities under stress at high-temperatures. Acta Metallurgica 25, 221–230.

Newcomb, S.A., Tressler, R.E., 1993. Slow crack-growth in sapphire fibers at 800-degrees to 1500-degrees-C. Journal of the American Ceramic Society 76, 2505–2512.

Nichols, F.A., 1976. Spheroidization of rod-shaped particles of finite length. Journal of Materials Science 11, 1077–1082.

Osher, S., Sethian, J.A., 1988. Fronts propagating with curvature-dependent speed – algorithms based on Hamilton–Jacobi formulations. Journal of Computational Physics 79, 12–49.

Patra, M., Karttunen, M., 2006. Stencils with isotropic discretization error for differential operators. Numerical Methods for Partial Differential Equations 22, 936–953.

Peng, D.P., Merriman, B., Osher, S., Zhao, H.K., Kang, M.J., 1999. A PDE-based fast local level set method. Journal of Computational Physics 155, 410–438.

Riege, S.P., Hunt, A.W., Prybyla, J.A., 1995. Real-time TEM studies of electromigration in submicron aluminum runners. In: Materials Reliability In Microelectronics V, vol. 391, pp. 249–258.

Salac, D., Lu, W., 2006. Design nanocrack patterns in heterogeneous films. Nanotechnology 17, 5185–5191.

Sethian, J.A., Smereka, P., 2003. Level set methods for fluid interfaces. Annual Review of Fluid Mechanics 35, 341–372.

Siegel, M., Miksis, M.J., Voorhees, P.W., 2004. Evolution of material voids for highly anisotropic surface energy. Journal of the Mechanics and Physics of Solids 52, 1319–1353.

Smereka, P., 2003. Semi-implicit level set methods for curvature and surface diffusion motion. Journal of Scientific Computing 19, 439–456.

Stahlmecke, B., zu Heringdorf, F.J.M., Chelaru, L.I., Horn-von Hoegen, M., Dumpich, G., Roos, K.R., 2006. Electromigration in self-organized single-crystalline silver nanowires. Applied Physics Letters, 88.

Stevens, R.N., Dutton, R., 1971. Propagation of Griffith cracks at high temperatures by mass transport processes. Materials Science and Engineering 8, 220–234.

Suo, Z., Hong, W., 2004. Programmable motion and patterning of molecules on solid surfaces. Proceedings of the National Academy of Sciences of the United States of America 101, 7874–7879.

Tvergaard, V., Hutchinson, J.W., 2002. Two mechanisms of ductile fracture: void by void growth versus multiple void interaction. International Journal of Solids and Structures 39, 3581–3597.

Vandervorst, H.A., 1992. Bi-Cgstab – a fast and smoothly converging variant of Bi-Cg for the solution of nonsymmetric linear-systems. Siam Journal on Scientific and Statistical Computing 13, 631–644.

Wang, W.Q., Suo, Z., 1996. A simulation of electromigration-induced transgranular slits. Journal of Applied Physics 79, 2394–2403.

Wang, W.Q., Suo, Z., 1997. Shape change of a pore in a stressed solid via surface diffusion motivated by surface and elastic energy variation. Journal of the Mechanics and Physics of Solids 45, 709–729.

Wu, C.H., 1999. The effect of surface stress on the configurational equilibrium of voids and cracks. Journal of the Mechanics and Physics of Solids 47, 2469–2492.

Wu, C.H., Hsu, J., Chen, C.H., 1998. The effect of surface stress on the stability of surfaces of stressed solids. Acta Materialia 46, 3755–3760.

Yang, F.Q., 2006. Stress-induced surface instability of an elastic layer. Mechanics of Materials 38, 111–118.

Yu, H.C., Lu, W., 2005. Dynamics of the self-assembly of nanovoids and nanobubbles in solids. Acta Materialia 53, 1799–1807.